

## Preparation of Highly-Active Oxygen Reduction Reaction Catalyst by Direct Co-Pyrolysis of Biomass with KOH

Weimin Cao<sup>1,\*</sup>, Bingjia Wang<sup>1</sup>, Yinpan Xia<sup>1</sup>, Wei Zhou<sup>1</sup>, Jia Zhang<sup>2</sup>, Ran Wen<sup>2</sup>,  
Yi Jia<sup>3</sup>, Qiang Liu<sup>2,\*</sup>

<sup>1</sup> College of Sciences, Shanghai University, No. 99 Shangda Rd., Shanghai 200444, P. R. China

<sup>2</sup> School of Environmental and Chemical Engineering, Shanghai University, No. 333 Nanchen Rd., Shanghai 200444, P. R. China

<sup>3</sup> Queensland Micro- and Nanotechnology Centre, Griffith University, Nathan Campus, Queensland 4111, Australia.

\*E-mail: [cwm213@staff.shu.edu.cn](mailto:cwm213@staff.shu.edu.cn), [qliu@shu.edu.cn](mailto:qliu@shu.edu.cn)

Received: 4 September 2018 / Accepted: 18 October 2018 / Published: 30 November 2018

---

In this work, we developed a cost-effective, facile approach to obtain nitrogen self-doped porous biomass-derived carbon catalyst by direct co-pyrolysis of corn straw biomass with KOH. Through characterization, the obtained catalyst possesses a quite high BET surface area up to 1461.36 m<sup>2</sup> g<sup>-1</sup> and significant pyrrolic-N content. Electrochemical test demonstrated that nitrogen self-doped porous carbon exhibits an excellent electrocatalytic activity for oxygen reduction reaction (ORR) in alkaline media, with onset potential of -0.06 V (vs Hg/HgO) and current density of -3.42 mA cm<sup>-2</sup>, which is comparable to 20% Pt/C catalyst. More importantly, obtained catalyst shows high stability and durability towards ORR reaction. Our results demonstrated that the co-pyrolysis process is a promising route for economical and sustainable utilization of biomass towards the effective metal-free ORR catalysts for alkaline fuel cell.

---

**Keywords:** biomass, KOH, ORR catalyst, co-pyrolysis

### 1. INTRODUCTION

Due to the benefits of cleanliness and high efficiency, fuel cell is considered to be one of the most promising technology to cope with future crisis on the generation of clean energy. The kinetics of oxygen-reduction reaction (ORR) at cathode is widely accepted as the most crucial factor that affects the performance of fuel cells [1-3]. So far, the reported high-performance electro-catalysts almost exclusively relied on Pt-based electro-catalysts [4-6]. However, the drawbacks of high cost, poor stability and low methanol tolerance of Pt catalysts [7] greatly restrict the wide application of fuel cell.

Therefore, developing high efficiency, low cost and precious metal free ORR electro-catalyst is paramount for future commercialization of fuel cell technology.

Recent investigations revealed that nitrogen doped carbon materials, such as N doped graphene [8-10], reduced graphene oxide [11], and ordered mesoporous carbon [12,13] show great potentials on ORR at fuel cell cathode. These metal-free carbonaceous catalysts attracted intensive interests from researchers due to the advantages of superior electro-catalytic activity and long durability. However, the synthetic process of these N doped catalysts is substantially complicated and usually involve poisonous nitrogen precursors such as ethylenediamine [14], tripolycyanamide [15], pyridine [16,17] and ammonia [18], which are harmful to human health. Clearly, exploring alternative precursor and new route for producing highly active ORR catalyst are urgently required.

Biomass is an attractive ORR catalyst precursor which is rich in carbon, environmentally friendly, readily available and renewable. Previous work indicated that charring materials obtained from oxygen free thermal pyrolysis of different forms of biomass, such as cotton [19], pollen grain [20], sawdust [21], silk [22], pulse flour [23], okara [24] and *Typha orientalis* [25] presented excellent ORR performance owing to the benefits of high porosity and surface area. The featured porous structure is supposed to facilitate high mass transfer fluxes and promote the contact between reactants and catalytic sites in two-dimension thin films or nanosheets in biomass-derived carbon.

In light of the importance of porosity of carbon electrocatalyst on ORR, some activation reagents are usually employed to develop pore structure in catalyst. For example, Zhao et al [26] using KOH as post-active agent to increase specific surface area and micropore content in a three-dimensional (3D) hierarchical porous carbon catalyst derived from *Artemia* cyst shell. Liu et al [27] preloaded  $ZnCl_2$  on soybean biomass as an activator to prepare high performance ORR catalyst with significant BET surface area (up to  $949\text{ m}^2\text{ g}^{-1}$ ). However, these modified synthesis methods usually contained tedious steps such as pre-impregnation of activator on biomass, post-activation of carbonized biomass, or multistage heating program, leading to complicated processes for catalyst preparation.

In this work, we use corn straw, a common agricultural bio-waste as a carbon source to develop a simple, low-cost and readily scalable approach for the synthesis of porous carbon-based catalyst by direct pyrolysis of biomass with KOH at controlled temperature. The resulting sample exhibited a high BET surface area and hierarchical porous distribution. Electrochemical measurements of this porous carbon demonstrated distinguished catalytic ability and stability towards ORR in alkaline solution, which was comparable to commercial Pt/C catalysts. Our co-pyrolysis approach can substantially simplify the synthesis process and reduce thermal treatment duration of biomass-derived ORR catalyst.

## 2. EXPERIMENTAL MATERIALS AND METHODS

Corn stalk used in this experiment was collected from Chongming Island, Shanghai, China. Obtained biomass was washed extensively by deionized water to remove impurities such as dusts and air-dried for days. Before pyrolysis, raw biomass was cut into pieces, ground to powder in a mortar, screened by 100 mesh sieve and oven-dried at  $105\text{ }^\circ\text{C}$  for 24 h. In a typical pyrolysis run, 5.0 g biomass was heated in a tube furnace at  $850\text{ }^\circ\text{C}$  under  $N_2$  flow ( $100\text{ mL/min}$ ) for 30 min. After cooling to room

temperature under N<sub>2</sub> gas, the carbonized product was alternately rinsed with 0.05 M HCl and 0.05 M NaOH to remove metal deposits and other impurities. The product of pyrolysis (marked with BC) was further washed with DI-water until constant pH and dried in an oven at 80 °C for future use. KOH activated catalyst was prepared by direct co-pyrolysis of the mixture of biomass powder and potassium hydroxide (1:1 by weight) under identical carbonization condition with BC and are labeled as BC-K-*t*, where *t* denoted pyrolysis time (i.e. 0.5, 1 h).

BET analysis of sample was performed by a Micromeritics ASAP 2020 using N<sub>2</sub> as adsorbate at -195.74 °C. Infrared spectra were collected by a Thermo Scientific FTIR 380 spectrometer at wave numbers of 400 - 4000 cm<sup>-1</sup> with each sample mixed with KBr at a ratio of 1:100 (w/w). Surface morphology of sample was characterized by a scanning electron microscope (JEOL JSM6700) equipped with an energy dispersive spectroscopy detector and a high-resolution transmission electron microscope (HRTEM, JEOL JEM-2010). XPS (ESCALAB 250 Xi, USA) was used to determine elemental composition and chemical state of elements on sample surface. The structure of biochar was characterized by X-ray powder diffraction (XRD) by a D/max-2500 X-ray diffractometer with Cu-*k* $\alpha$  radiation (40 Kv, 250 Ma,  $k = 0.1789$  nm) at a scanning speed of 4 °/min and a scan  $2\theta$  range of 5 - 80°.

Electrochemical experiment was conducted on a CHI660A electrochemical workstation (CH instrument Co., China) with a three-electrode cell equipped with gas-flow system. Counter and reference electrodes used in this experiment were a platinum sheet and a Hg/HgO (2 M KOH solution) electrode, respectively. Working electrode was a glassy carbon electrode with 3 mm in diameter. In a typical electrochemical test, 5.0 mg of biochar was added into 2 mL ethanol and 10  $\mu$ L Nafion solution (1 wt%, Alfa Aesar) and sonicated for 30 min to form a well-dispersed ink. Afterward, 10  $\mu$ L dispersion was evenly spread onto the surface of glassy carbon electrode and dried at room temperature for 2 h to form a catalyst thin film. Commercial Pt/C catalyst was loaded onto the surface of electrode by the same method and used as reference in this experiment. For ORR measurement, alkaline electrolyte (0.1 M KOH) was purged with high-purity N<sub>2</sub> or O<sub>2</sub> gas for 30 min to ensure gas saturated. Cyclic voltammetry (CV) measurements were conducted over the potential range of -0.8 to +0.2 V (*vs* Hg/HgO) with a scan rate of 50 mV s<sup>-1</sup>. Linear sweep voltammetry (LSV) measurements were conducted at a scan rate of 50 mV s<sup>-1</sup>. The accelerated durability test (ADT) [28] of sample was performed in N<sub>2</sub>-saturated 0.1 M KOH at the potential range from -0.8 to 0.2 V with a scan rate of 50 mV s<sup>-1</sup>. Sample stability was also evaluated by current *vs.* time (*i-t*) chronoamperometric response at a constant potential of -0.35 V in O<sub>2</sub>-saturated 0.1 M KOH. All tests were carried out at ambient temperature and airtight condition.

### 3. RESULTS AND DISCUSSION

Morphology and structure of samples were characterized to identify the effect of KOH co-pyrolysis on catalyst. Scanning electron microscopy (SEM) micrograph reveals BC (Fig. S1a) consisted of a lot of carbonaceous fragments which are irregular in shape and free of pore on surface. In contrast to BC, BC-K-0.5 (Fig. 1a) and BC-K-1 (Fig. S1b) were abundant with hierarchical porous structure on surface, suggesting these samples owned large specific surface area. High resolution SEM image (Fig. 1b) further confirms the highly ordered porous structure of BC-K-0.5, which featured with

interconnected macro-pores (1-2  $\mu\text{m}$  in diameter) separated by 0.5-2  $\mu\text{m}$  carbon wall. These results demonstrate the co-pyrolysis of biomass with KOH is effective in establishing and developing three-dimensionally ordered structure inside catalyst. It is worthy noted that BC-K-0.5 (Fig. 1a) shows more excellent structure than BC-K-1 because the latter presents more fractures and blocked channels (Fig. S1b). The break and collapse in carbon skeleton of BC-K-1 reveals the activation of KOH happened excessively with the increase in heating duration, and also highlights the potential in shortening thermal treatment time in the co-pyrolysis process.

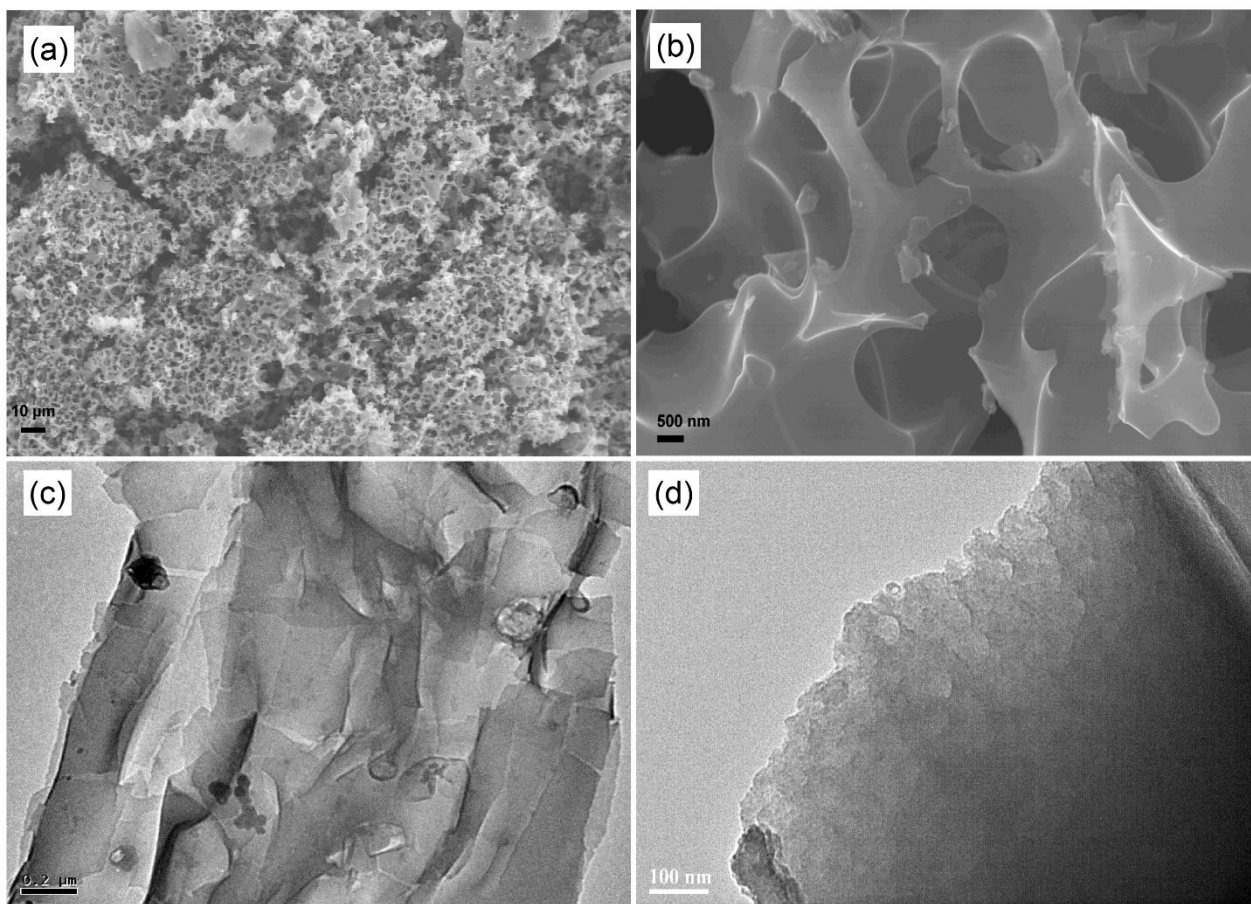


**Figure 1.** (a) SEM image, (b) HRSEM image, (c) TEM image and (d) HRTEM image of BC-K-0.5

Morphology and structure of BC-K-0.5 were further detected by transmission electron microscope (TEM) analysis. It can be clearly seen that BC-K-0.5 was rich in smooth graphene-like structure with several micrometers in size (Fig 1c). High resolution TEM images also reveals that BC-K-0.5 sample was composed of highly curved graphitic layers. It is well known that graphene possesses excellent electrical conductivity which is favorable for fast and smooth electron transfer [10]. Therefore, it can be expected that porous channels in BC-K-0.5 is beneficial for electrolyte infiltrating into catalyst and further contacting with active sites on catalyst. Besides, published works also reported that open edge sites and higher curvatures on carbon catalyst are favorable for ORR because these structures may

assist oxygen molecule to conveniently and effectively access to the electrocatalytic active sites produced from nitrogen doping [29, 30].

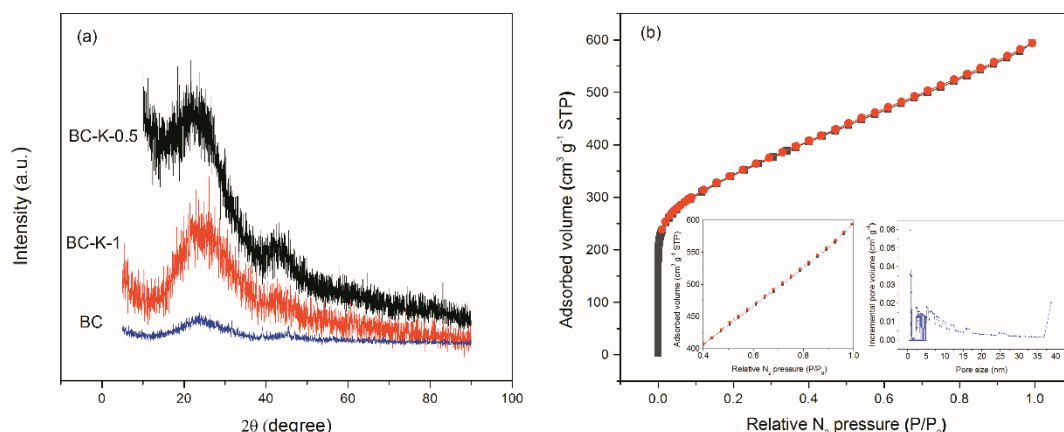


**Figure 2.** (a) XRD patterns of BC and BC-K-0.5 and (b) Nitrogen adsorption-desorption isotherms at 77 K and DFT pore-size distribution (inset) of BC-K-0.5

Fig. 2a shows the X-ray diffraction (XRD) patterns of three samples. As can be observed, these samples exhibited two pronounced peaks around  $23.6^\circ$  and  $43.8^\circ$ , which correspond to (002) and (100) lattice planes of a typical turbostratic carbon, respectively. This result demonstrates the formation of graphitic carbon in all samples [31]. However, based on remarkably strengthened and broadened characteristic bands of turbostratic structures in BC-K-0.5 (as revealed in Fig. 2a), it can be inferred that a higher degree of structural alignment is more easily formed at co-pyrolysis process.

$N_2$  adsorption-desorption isotherm was used to analyze the porosity and pore-size distribution of BC-K-0.5. According to Fig. 2b, the occurrence of hysteresis loop in high pressure range proves BC-K-0.5 was abundant with mesopores, while the sharp increase at low pressure indicates a certain amount of micropores also existed in this sample. Furthermore, the pore size distribution (Fig. 2b inset) calculated *via* density functional theory (DFT) method declared the prevalence of pores ranging from 1 to 40 nm in size, demonstrating a larger number of micropores and mesopores within catalysts, which is in conformity with SEM and TEM results of BC-K-0.5. Specific surface areas of three samples are presented in Table 1.

**Table 1.** BET surface area and elemental analysis of BC, BC-HN and BC-K

Samples	BET surface area ( $m^2 g^{-1}$ )	C (%)	N (%)	H (%)	O <sup>a</sup> (%)
BC	33.06	75.01	2.13	1.38	21.48
BC-K-1	955.46	85.51	0.77	0.8	12.92
BC-K-0.5	1461.36	79.4	1.15	5.73	13.72

<sup>a</sup> assumed from the remainder of 100%, which didn't consider ash.

It is quite clear that the specific surface area of BC-K-0.5 ( $1461.36 \text{ m}^2 \text{ g}^{-1}$ ) is much higher than the other two samples, which is in consistence with the electron microscope images. In fact, BC-K-0.5 produced a superior total pore volume up to  $0.918 \text{ cm}^3 \text{ g}^{-1}$ , of which micropores volume is  $0.520 \text{ cm}^3 \text{ g}^{-1}$ . The high surface area of BC-K-0.5 allows the catalyst possess high density of active sites. In addition, the abundance in mesoporous structures are beneficial to the diffusion of ORR related species [32-34].

The result of element analysis of each sample was also compiled in Table 1. It can be founded that nitrogen doping in samples were 2.13 at%, 1.15 at% and 0.77 at% for BC, BC-K-0.5 and BC-K-1, respectively (Table 1). Note that no extra N source was introduced in the synthetic process, these nitrogen contents come exclusively from inherent N species of raw biomass. High N contents is desirable for catalyst for that previous experiment revealed that carbon atoms adjacent to nitrogen have high positive charge density which can lead to increased  $\text{O}_2$  adsorption and thus accelerated ORR [9-10].

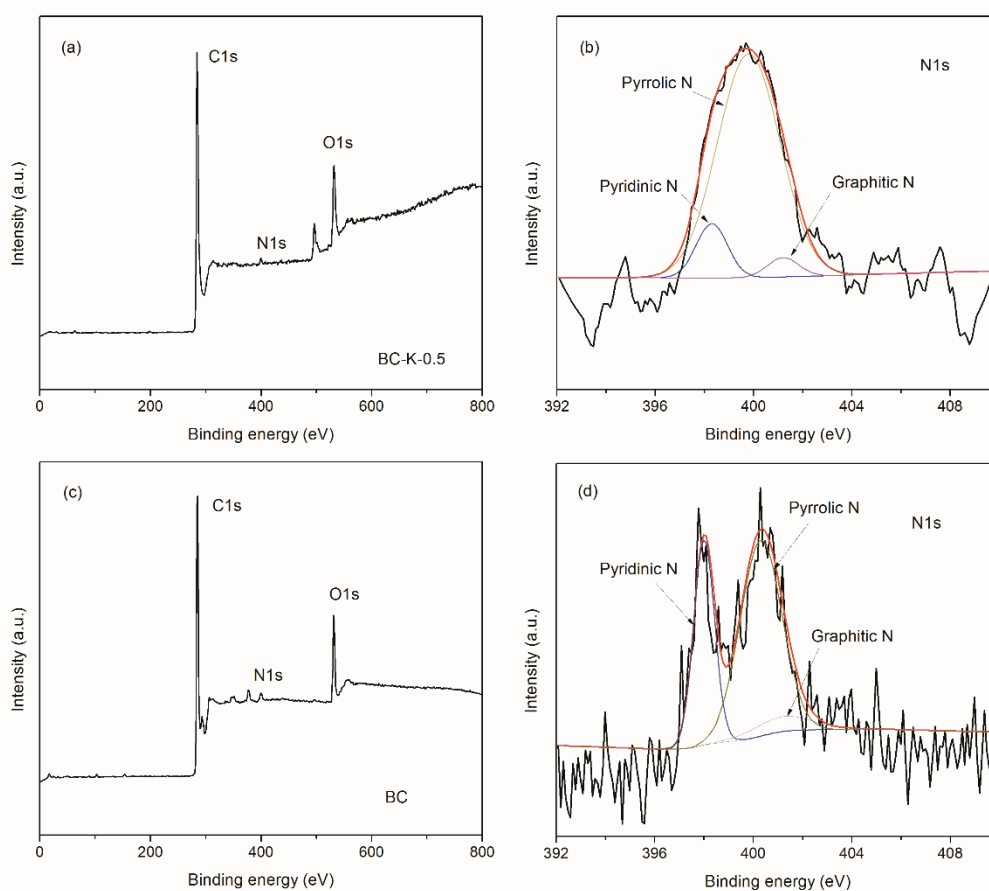


**Figure 3.** XPS spectra of surface chemical composition of (a) BC-K-0.5 and (c) BC and high-resolution N1s spectra of (b) BC-K-0.5 and (d) BC

X-ray photoelectron spectroscopy (XPS) analysis was implemented to further indentify elemental chemical characteristics of samples, with particular emphasis on the bonding configuration of nitrogen. Clearly, C 1s (c.a. 284 eV), O 1s (c.a. 532 eV) and N 1s (c.a. 400 eV) spectra were detected in each sample, proving that these samples are indeed nitrogen self-doping carbon materials. High-

resolution N 1s spectra of three samples were deconvoluted to clarify N species presented in catalysts. As illustrated in Fig. 3b and d, three major types of nitrogen group were identified and ascribed to pyridinic-N ( $398.4\pm 0.3$  eV), pyrrolic-N ( $400.1\pm 0.3$  eV) and quaternary or graphitic-N ( $401.2\pm 0.3$  eV), respectively [35-37]. The percentages of total nitrogen and each nitrogen species in BC and BC-K-0.5 were quantified by integrating the peak area of corresponding signal and the results are shown in Fig. 4. Total nitrogen contents in BC-K-0.5 and BC surface are 4.21% and 2.81%, respectively, which are much higher than N contents determined by elementary analysis, especially for BC-K-0.5. It is inferred that high specific surface area makes more nitrogen contained groups exposed on the surface of samples. With regard to detailed N species, it is intuitive to see that pyrrolic-N and pyridinic-N are in the majority of N groups in these two samples. In terms of pyrrolic-N, 1.58% for BC, 3.68% for BC-K-0.5, with the latter one presenting higher pyrrolic-N content. In addition, BC-K-0.5 has lower content of graphitic-N (only 0.147%).

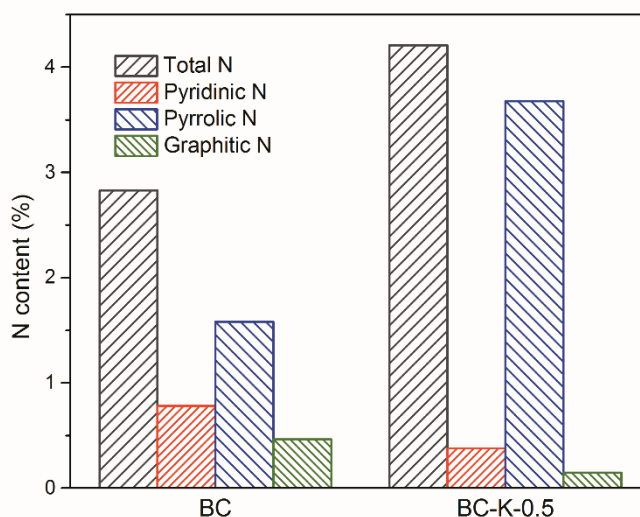


**Figure 4.** Nitrogen contents in BC and BC-K-0.5

ORR performance of N-doped carbon catalyst is strongly dependent on the nitrogen configurations. However, there still existed controversial viewpoints on the detailed catalytically active sites of nitrogen functionality. Several studies reported that pyridinic-N and pyrrolic-N have planar structure without torsion angle of C-N bond for planar  $sp^2$ -hybridized orbital, which are active to ORR [38-40]. Recent investigations revealed pyrrolic N is more crucial for ORR performance of nitrogen-doped catalysts because the withdraw effect on electron by pyrrolic N is more intense than pyridinic-N so that the former can activate adjacent carbon atoms to show higher affinity to oxygen molecules [41, 42]. On the contrary, graphitic-N presents a three dimensional (3D) structure which is not desired for ORR since carbon with quaternary-N presents tetrahedral  $sp^3$ -hybridized N which forms non-uniform structure [39]. In light of significant high pyrrolic-N content while low graphitic-N content in BC-K-0.5, it can be anticipated that this sample has better catalytic performance.

To confirm this speculation, electrocatalytic performance of BC-K-0.5 towards oxygen reduction reaction was tested through cyclic voltammetry (CV). From Fig. 5, under nitrogen atmosphere, a quasi-

rectangle voltammogram without any redox peak appears for all samples. After oxygen dissolved in electrolyte, a well-defined oxygen reduction cathodic peak can be observed obviously from Fig. 5 a-e, demonstrating these three samples are active to ORR. As special for peak potential, BC-K-0.5 exhibited a more positive shift of -0.16 V in contrast to BC-K-1 (-0.36 V) and BC (-0.37 V), which is also close to Pt-C (-0.07 V). It is interesting to find that the current of BC-K-0.5 is much higher than others and some reported samples (see Table S1 in Supporting material) [10, 43-46], which means this sample owned excellent electrical conductivity and also reveals higher electrocatalysis activity towards ORR.

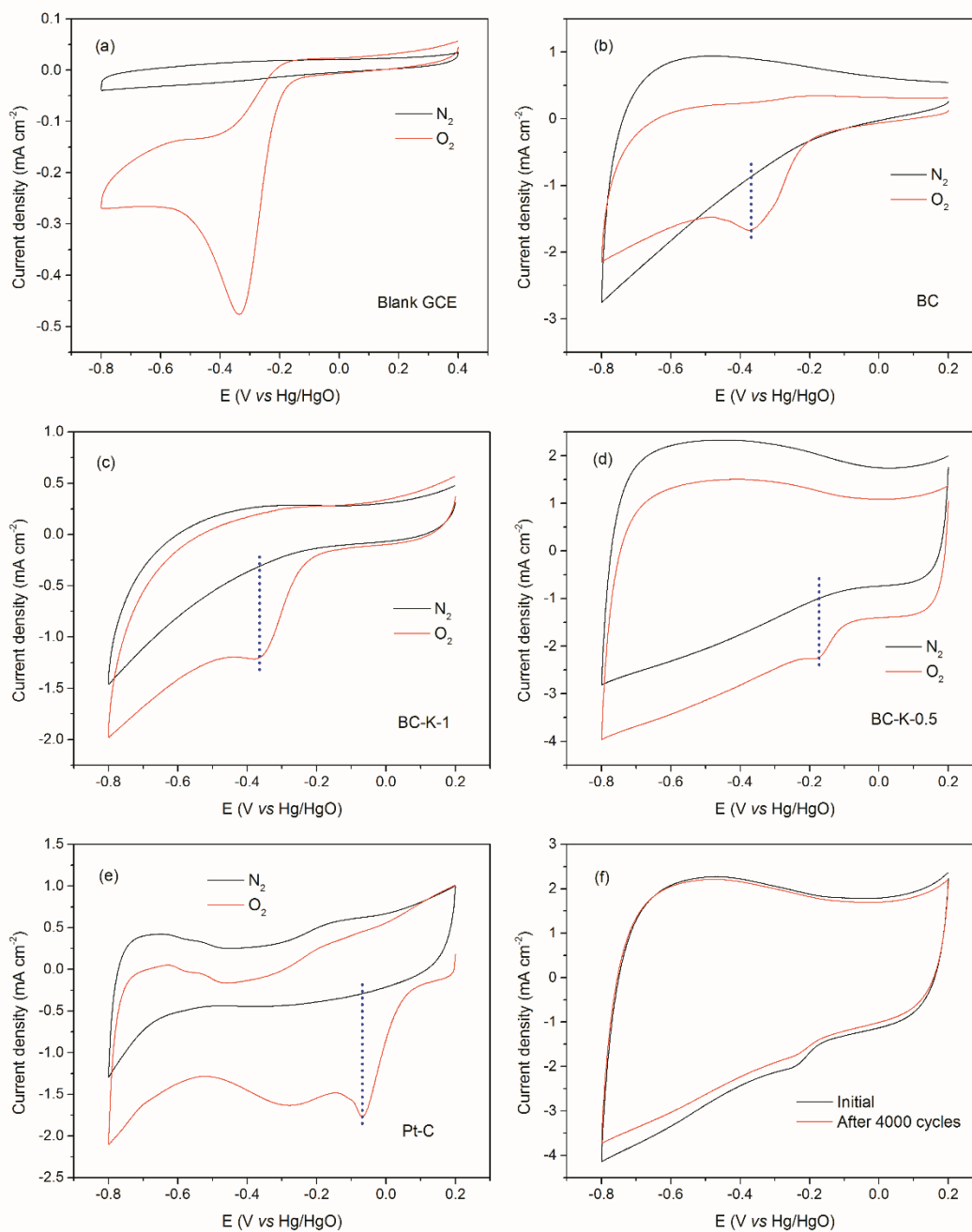


**Figure 5.** Cyclic voltammograms of (a) blank glass carbon, (b) BC, (c) BC-K-1, (d) BC-K-0.5 and (e) 20% Pt/C in N<sub>2</sub> and O<sub>2</sub>-saturated 0.1 M KOH and (f) BC-K-0.5 before and after ADT

Electrochemical durability in alkaline media is another important factor to evaluate the performance of ORR catalyst. The durability of BC-K-0.5 was first evaluated by comparing the changes in CV curves before and after the ADTs. The sample was continuously cycled with a scan rate of  $50 \text{ mV s}^{-1}$  in nitrogen saturated  $0.1 \text{ M KOH}$  for 4000 times. As can be observed from Fig. 5f, after 4000 cycles, the reduction in ORR activity of BC-K-0.5 is negligible in contrast to fresh sample.

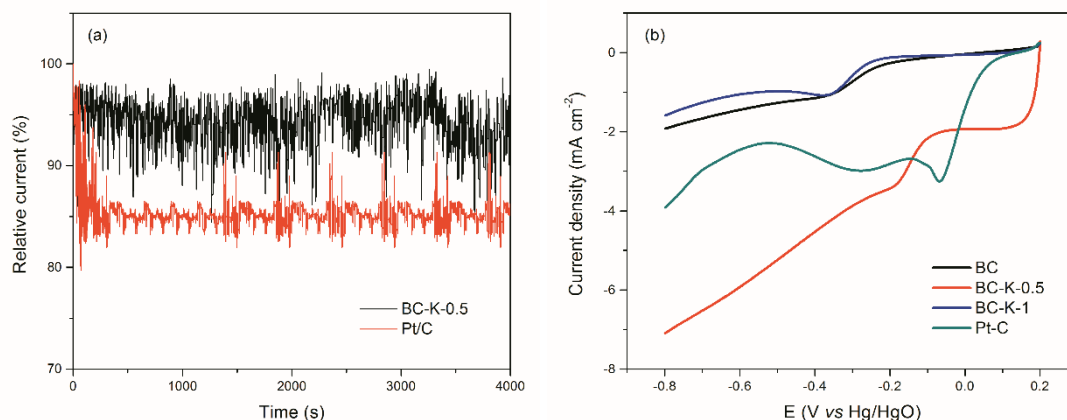
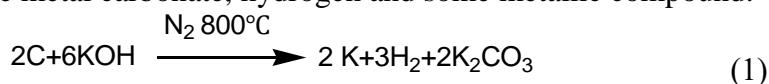


**Figure 6.** (a) Current-time ( $i-t$ ) responses of BC-K-0.5 and Pt/C at  $-0.35 \text{ V vs Hg/HgO}$  in  $\text{O}_2$ -saturated  $0.1 \text{ M KOH}$  solution for 4000 s and (b) Linear sweep voltammetry (LSV) measurement of all samples

To further confirm the stability of catalyst, current-time responses of BC-K-0.5 and Pt/C were carried out and the profiles are shown in Fig. 6a. As seen, after 4000 s of continuous operation, ORR activity of BC-K-0.5 maintained around 92%, which is a little higher than Pt/C (about 85%) in the same condition, revealing BC-K-0.5 possesses better stability in contrast to Pt/C. Linear sweep voltammetry (LSV) in  $\text{O}_2$ -saturated  $0.1 \text{ M KOH}$  solution at room temperature was also tested and results are compiled in Fig. 6b. It is worth noting that BC-K-0.5 had a rapid decline in  $0.2 \text{ V}$ , which is electric double layer current rather than oxygen reduction current. For BC-K-0.5, the onset potential ( $E_0 = -0.06 \text{ V}$ ) and current density ( $j = -3.42 \text{ mA cm}^{-2}$ ) is much higher than that of BC-K-1 ( $E_0 = -0.11 \text{ V}$ ,  $j = -0.87 \text{ mA cm}^{-2}$ ) and BC ( $E_0 = -0.13 \text{ V}$ ,  $j = -1.09 \text{ mA cm}^{-2}$ ). Compared with Pt/C ( $E_0 = 0.09 \text{ V}$ ,  $j = -3.25 \text{ mA cm}^{-2}$ ) catalysis, BC-K-0.5 exhibited slightly negative onset potential but a little higher current density. Surprisingly, it can be found that catalytic performance of BC-K-1 is close to KOH free sample, which is substantially lower than BC-K-0.5. This finding suggests thermal treating time in KOH co-pyrolysis process should be carefully controlled to avoid over activation. Based on above result, BC-K-0.5 exhibits distinguished ORR electrocatalytic performance and embodies in positive onset and great current density. The better ORR performance should be attributed to large specific surface area and high and pyrrolic-N content.

The activation mechanism of KOH on carbon-based ORR catalyst has been well illustrated [47, 48]. As shown in reaction (1), carbon atoms in precursor can react with KOH at high temperature to produce metal carbonate, hydrogen and some metallic compound.



With the progress of reaction, micropores in carbon will gradually develop due to the release of volatiles at 500 - 700 °C. It was reported that the release of CO<sub>2</sub> from K<sub>2</sub>CO<sub>3</sub> (above 700 °C) is particularly important for KOH activation because it can open up closed pores and expand existing micropores, and as a result develop hierarchical porous structures in catalyst [48]. In addition, metallic potassium may also improve pore volume and BET surface area of carbon-based catalyst [49, 50].

In contrast to common activation method *via* KOH pre-impregnation approach [26, 51, 52], the direct co-pyrolysis of biomass with KOH has the following advantages: (1) greatly simplify the synthesis procedures of catalyst, for example, the impregnation of KOH solution on feedstock and subsequent drying steps are not required anymore; (2) significantly reduce the pyrolysis duration of biomass, which is much desired because lots of energy can be saved; (3) have the potential to tune the distribution of pore sizes, for example, developing more mesoporous structure and increasing the size of mesoporous range *via* proper control of the amount and granularity of KOH. However, as revealed in this experiment, the ratio of biomass and KOH as well as thermal treatment conditions should be thoroughly explored and carefully controlled for particular biomass precursor to avoid over-activation.

#### 4. CONCLUSIONS

Nitrogen self-doped porous graphene-like carbon was synthesized *via* a simple, mild and one-step procedure using a common kind of waste biomass - corn straw as both the carbon and nitrogen source based on KOH activation. The obtained catalyst presented a considerably high surface area (up to 1461.36 m<sup>2</sup> g<sup>-1</sup>) and showed prominent ORR performance, which is not inferior to 20% commercial Pt/C catalysts, especially on the current density. The co-pyrolysis method can greatly simplify the preparation process and reduce thermal treating time of catalyst. The results indicated that porous nitrogen-doped graphene *via* one-step pyrolysis of corn straw with KOH is a promising non-metal ORR electrocatalyst material for low temperature fuel cell in alkaline electrolyte.

#### SUPPORTING MATERIAL:

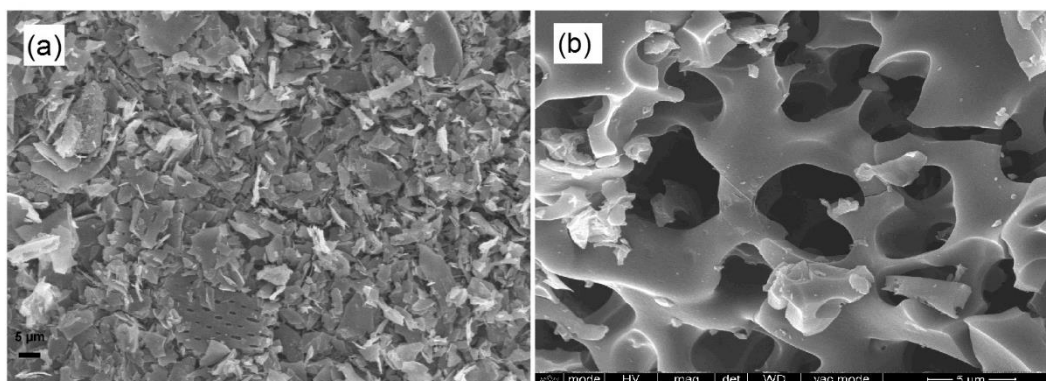


**Figure S1.** SEM images of (a) BC and (b) BC-K-1.

**Table S1** The catalytic properties of ORR catalyst prepared by difference methods.

Authors	Preparation method	N content	Limiting current density	Onset potential	High stability	Reference
Wong et al	Pyrolysis of GO and PANI	2.4 at%	8.9 mA/ cm <sup>2</sup>	-0.35V (vs Ag/AgCl)	Yes	[10]
Liu et al	Pyrolysis of pig bones and KOH solution activation	7.9 at%	-	0.58V (vs SCE)	Yes	[43]
Wang et al	pre-impregnation-pyrolysis	1.89 at%	-	0.946V (vs RHE)	Yes	[44]
Zhang et al	Pyrolysis Corncob	3.58 at%	-	-0.13V (vs Ag/AgCl)	Yes	[45]
Chen et al	Hydrothermal flower spikes, freeze drying and annealing inNH <sub>3</sub>	9.1 at%	-	0.8V (vs RHE)	Yes	[46]
This work	Direct Co-Pyrolysis of Biomass with KOH	4.21 at%	3.42 mA/ cm <sup>2</sup>	-0.06V(vs Hg/ HgO)	Yes	

#### ACKNOWLEDGEMENTS

This work was financially supported by National Nature Science Foundation of China (NSFC) (No. 415272349).

#### References

1. S. Wang, S.P. Jiang, *Natl. Sci. Rev.*, 4(2017) 163.
2. M. K. Debe, *Nature*, 486 (2012) 43.
3. R. Cao, R. Thapa, H. Kim, X. Xu, M. G. Kim, Q. Li, N. Park, and M. L. J. Cho, *Nat. Commun.*, 4 (2013) 2076.
4. B. Cai, R. Hübner, and K. Sasaki, *Angew. Chem. Int. Ed.*, 57 (2018) 2963.
5. J. Liu, M. Jiao, and L. Lu, *Nat. Commun.*, 8 (2017) 15938.
6. S. Sui, X. Wang, and X. Zhou, *J. Mater. Chem. A.*, 5 (2017) 1808.
7. G. Wu, P. Zelenay, *Chem. Res.*, 46 (2013) 1878.
8. M. Borghei, N. Laocharoen, E. Kibena-Pöldsepp, L.S. Johansson, J. Campbell, E. Kauppinen, K. Tammeveski, and O.J. Rojas, *Appl Catal B-Environ.*, 204 (2017) 394.
9. X. Li, Y. Yao, and J. Liu, *Int. J. Hydrogen Energy*, 42 (2017) 19903.
10. Z. Lin, G. H. Waller, Y. Liu, M. Liu, and C. Wong, *Carbon*, 53 (2013) 130.
11. M.D. Meganathan, S. Mao, and T. Huang, *J. Mater. Chem. A.*, 5 (2017) 2972.
12. K. Kwon, Y. J. Sa, J. Y. Cheon, and S. H. Joo, *Langmuir*, 28 (2012) 991.
13. W. Yang, T. Fellingner, and M. Antonietti, *J. Am. Chem. Soc.*, 133 (2011) 206.
14. S. Yang, X. Feng, X. Wang, and K. Müllen, *Angew. Chem. Int. Ed.*, 50, (2011), 5339.
15. J. Shi, Y. Wang, W. Du, and Z. Hou, *Carbon*, 99 (2016) 330.
16. S. Chen, J. Bi, Y. Zhao, L. Yang, C. Zhang, Y. Ma, Q. Wu, X. Wang, and Z. Hu, *Adv. Mater.*, 24 (2012) 5593.
17. T. Sharifi, G. Hu, X. Jia, and T. Wågberg, *ACS Nano*, 6(2012), 8904.
18. F. Pan, Z. Cao, Q. Zhao, H. Liang, and J. Zhang, *J. Power Sources*, 272 (2014) 8.
19. G. Jiang, B. Peng, *Mater. Lett.*, 188 (2017) 33.
20. Y. Wang, Z. Liu, B. Han, Y. Huang, and G. Yang, *Langmuir*, 21 (2005) 10846.

21. M. Sevilla, C. Sanchís, and A. B. Fuertes, *J. Phys. Chem. C.*, 111 (2007) 9749.
22. T. Iwazaki, H. Yang, R. Obinata, W. Sugimoto, and Y. Takasu, *J. Power Sources*, 195 (2010) 5840.
23. R. Gokhale, S. M. Unni, D. Puthusseri, S. Kurungot, and S. Ogale, *Phys.Chem.Chem.Phys.*, 16 (2014) 4251.
24. R. f. Wang, H. Wang, T. Zhou, J. Key, Y. Ma, Z. Zhang, S. J. Q. Zhao and A Wang, *J. Power Sources*, 274 (2015) 741.
25. P. Chen, L.K. Wang, G. Wang, M.R. Gao, J. Ge, W.J. Yuan, Y.H. Shen, A.J. Xie and S. H. Yu, *Energy Environ. Sci.*, 7 (2014) 4095.
26. Y. Zhao, W. Ran, J. He, Y. Song, C. Zhang, D. Xiong, F. Gao, J. Wu, and Y. Xia, *ACS Appl. Mater. Interfaces*, 7 (2015) 1132.
27. F. Liu , H. Peng, X. Qiao, Z. Fu, P. Huang, and S. Liao, *Int. J. Hydrogen Energy*, 39 (2014) 10128.
28. K. Kwon, Y. J. Sa, J. Y. Cheon, and S. H. Joo, *Langmuir* ,28 (2012) 991.
29. K. N. Chaudhari, M. Y. Song, and J. Yu, *Small*, 10 (2014) 2625.
30. B. Frank, M. E. Schuster, R. Schölgl, and D. S. Su, *Angew. Chem. Int. Ed.*, 52 (2013) 2673.
31. C. Hu, Y. Xiao, Y. Zhao, N. Chen, Z. Zhang, M. Cao, and L. Qu, *Nanoscale*, 5 (2013) 2726.
32. W. Jiao, Z. R. Yang, X. W. Li, Q. J. Sun, and R. Z. Yang, *J. Mater. Chem. A.*, 1 (2013) 9889
33. H.W. Liang, W. Wei, Z. S. Wu, X. L. Feng, and M. Klaus, *J. Am. Chem. Soc.*,135 (2013) 16002.
34. W. J. Qian, F. X. Sun, Y. H. Xu, S. D. Wang, and F. Yang, *Energy Environ. Sci.*, 7 (2014) 379.
35. C. Guo, W. Liao, Z. Li, and C. Chen, *Carbon* , 85 (2015) 2.
36. Z. Liu, H. Nie, Z. Yang, J. Zhang, Z. Jin, Y. Lu, Z. Xiao, and S. Huang, *Nanoscale*, 5 (2013) 3283.
37. L. L. Zhang, X. Zhao, H. Ji, M. D. Stoller, L. Lai, S. Murali, S. McDonnell, B. Cleveger, R. M. Wallacec, and R. S. Ruoff, *Energy Environ. Sci.*, 5 (2012) 9618.
38. S. Yang, X. Feng, X. Wang, and K. M. Llen, *Angew. Chem. Int. Ed.*, 50 (2011) 5339.
39. W. Ding, Z. Wei, S. Chen, X. Qi, T. Yang, J. Hu, D. Wang, L. Wan, S. F. Alvi, and L. Li, *Angew. Chem. Int. Ed.*, 52 (2013) 11755.
40. K. Han, J. Shen, S. Hao, H. Ye, C. Wolverton, M. C. Kung, and H. H. Kung. *ChemSusChem.*, 7 (2014) 2545.
41. C. Guo, C. Chen, and Z. Luo, *J. Power Sources*, 245 (2014) 841.
42. C. Guo, W. Liao, and C. Chen, *J. Power Sources*, 269 (2014) 841.
43. H. Liu, Y. Cao, and F. Wang, *Electroanalysis*, 26 (2014) 1831.
44. R. Wang, H. Wang, and T Zhou, *J. Power Sources*, 274 (2015) 741.
45. M. Li, H. G. Zhang, T. F. Xiao, S. D. Wang, B. P. Zhang, D. Y. Chen, M. H. Su and J. F. Tang, *Electrochim Acta*, 283 (2018) 780.
46. P. Chen, L. K. Wang, and G Wang, *Energy & Environ. Sci.*, 7 (2014) 4095.
47. Y. Zhao, W. Ran, J. He, Y. Huang, Z. L. Lu, W. Liu, Y. Tang, L. Zhang, D. Gao, and F. Gao, *Small*, 11 (2015) 1310.
48. E. R. Ero, T. C. P. Azaí S A, D. C. S, A. Linares-Solano, and F. B. Guin, *Carbon*, 43 (2005) 786.
49. H. Teng, L. Hsu, *Ind. Eng. Chem. Res.*, 38 (1999) 2947.
50. B. Xing, G. Huang, and Z. Chen, *J. Solid State Electr.*, 21 (2017) 263.
51. J. Zhang, S. Y. Wu, X. Chen, P. Mu, and S. C. Wu , *J. Power Sources*, 271,(2014) 522.
52. H. Chen, D. Liu, Z. H. Shen, B. F. Bao, S. Y. Zhao, and L. M. Wu, *Electrochim Acta* ,180 (2015) 241